ICAST2014 #053

Design of an autonomous flap for load alleviation

Lars O. Bernhammer[1], Jurij Sodja[1], Moti Karpel[2], Roeland De Breuker[1]

[1] Faculty of Aerospace Engineering, Delft University of Technology, Delft, Netherlands
[2] Faculty of Aerospace Engineering, Technion Israel Institute of Technology, Haifa, Israel

Abstract

In this paper the design of an experimental, aeroelastic set-up for a novel load alleviation concept using trailing edge flaps is presented. These flaps are autonomous in terms of power supply, control and actuation, which is especially advantageous as complex wiring to connect the control surfaces is redundant. The flaps are free-floating and therefore vibrate in response to turbulence. The vibrations are converted to electricity through an electromagnetic device. The harvested energy is used to power both actuators and accelerometers.

Keywords: Autonomous flap, aeroelastic instability, load control

1. INTRODUCTION

The structural design of both aircraft wings and wind turbine blades are strongly driven by gust encounters or turbulence. A way to reduce the impact of these load cases is through active load alleviation. A suitable option are trailing edge flaps as they combine a wide frequency bandwidth with a high control authority on the lift coefficient and thereby on the loads that occur in the structure. One of the proposed implementations are so-called free-floating flaps (FFF). These flaps have first been investigated by Heinze and Karpel [1] who use a single FFF to control very flexible wings. Bernhammer et al. [2] have expanded this research on free-floating flaps to gust load alleviation and flutter suppression through controlling the flap by trailing edge tabs. Pustilnik and Karpel [3,4] expanded this work by investigating limit cycle oscillations.

While control of flap systems is a relatively well-established topic, the second element of an autonomous unit, energy harvesting, is less advanced. Harvesting energy from mechanical vibrations is a well-researched topic, however actively using aeroelastic instabilities is a relatively new field of research. Ground work has been done by Bryant and Garcia [5] and Bryant, Fang and Garcia [6] who extract energy from flutter of a cantilever bender with a free-floating flap. Park et al. [7,8] take a different approach by replacing the piezoelectric material that served as energy source for Bryant and Garcia [5] by an

electromagnetic approach. Aeroelastic instabilities are generated by means of vortex shedding form a T-shaped cantilever beam. The magnet is attached to the free tip and generates a magnetic field that induces currents in the coils that are placed in a non-rotating frame. Bernhammer, De Breuker and Karpel [9,10] followed this idea and advanced it to a stage of practical applicability for aerospace problems. Two FFFs are embedded in a wing structure. The flap rotation is translated into electricity by means of a dynamo.

2. CONCEPT OF THE AUTONOMOUS FLAP

The current design combines the functionality of the free-floating flap driven by the trailing edge tab with the energy harvester by Bernhammer, De Breuker and Karpel [9,10]. This concept is detailed in Figures 1 and 2. As shown in Figure 1, the autonomous flap unit consists of 6 parts. The flap serves as the top level component, which encloses the other subcomponents except for the trailing edge tab. The first loop is a traditional control system. A sensor (e.g. accelerometers) senses the motion of the wing-flap configuration. This can be a single sensor or an array of sensors. For the presented experiment, an accelerometer will be used, which is mounted close to the rotational axis as shown in Figure 2. The measured plunge acceleration obtained by this sensor is used as input to the controller, which is developed based on the aeroelastic state-space model. Alternatively, the controller can also be designed based on a system identification during the experiment. The controller determines a response to this motion signal. This signal is converted by an actuator into a deflection of the trailing edge flap. The loop is closed through the aerodynamic forces generated by the trailing edge tab, which drive the flap.

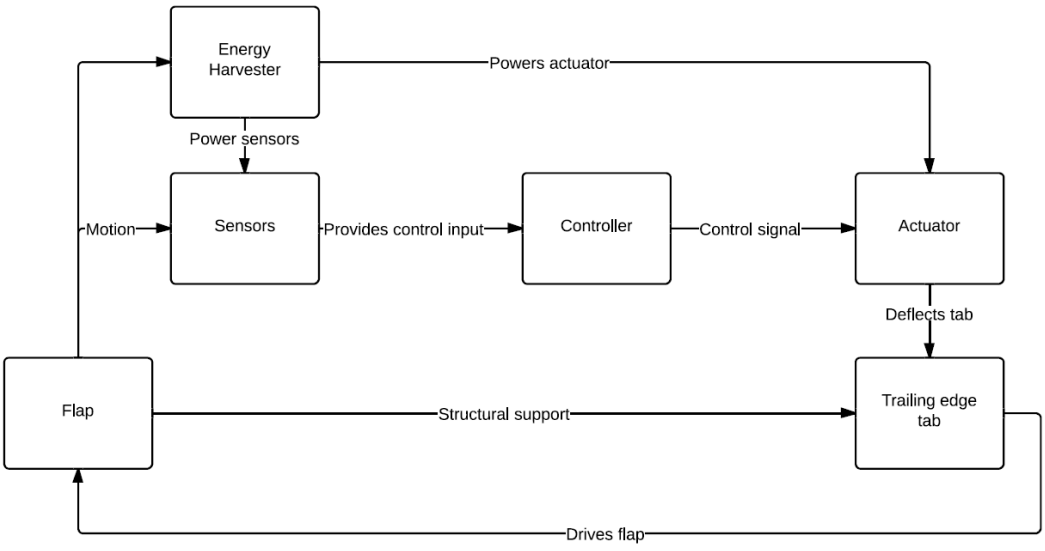

Figure 1. Flow chart of autonomous flap concept

Hence, the conventional control system is supplemented with an additional control loop to facilitate for control during the energy harvesting phase of the FFF. A dynamo converts mechanical power from the flap motion to electricity. This can be used either directly to power sensors and actuators or be stored in batteries for later usage. The energy harvesting is particularly effective, when the system is aeroelastically instable. It is therefore desired that the flap system will flutter. Limit cycle oscillations are a way to achieve sustained oscillations without being structurally destructive.

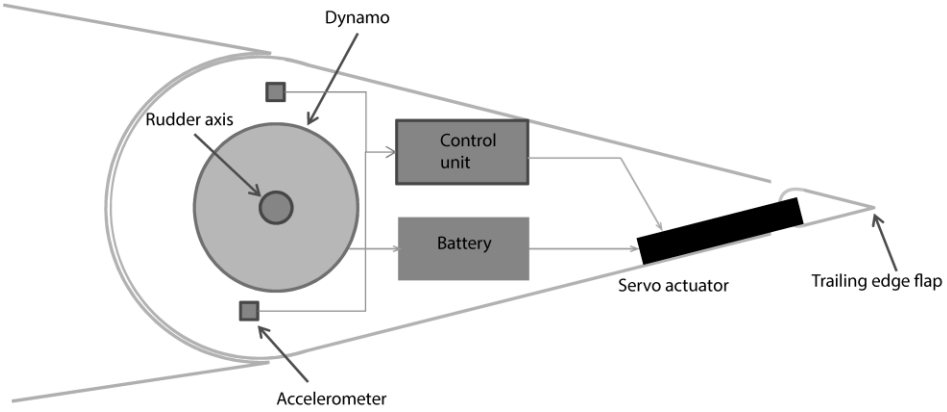

Figure 2. Schematic build-up of free-floating flap

3. AEROELASTIC TEST SET-UP

The autonomous flap concept is applied to an already existing aeroelastic test-set up of an airfoil that can undergo pitch and plunge motion and has a conventional flap. This experiment has been heavily validated using CFD data [11]. Especially, lift measurements agree excellently with numerical prediction where the difference is less than 5%. The test set-up of this experiment is shown in Figure 3. The wing model (F) is attached by springs to a frame built of sidewalls (C) connected by beams (D). This frame is mounted on a table (B), which can be adjusted to the height of the jet exit of the open test section (A). Struts (E) on both sides are used to increase the stiffness of the frame. Plunge and pitch motion of the wing are decoupled by having a global translating system (I) on which rotational springs are mounted that give an additional degree of freedom as shown in Figure 4. The side plates are guided by a rail system to prevent motion other than pure plunge. The properties of this set-up are given in Table 1.

Table 1 Properties of aeroelastic set-up

Width	Chord	Airfoil profile	Flap length	Plunge stiffness
1800mm	500mm	DU-96-W-180	100mm	8225N/m^2
Structural damping	Wing assembly mass	Wing mass	Side plate mass	First eigenfrequency

77.9kg/s	26.7kg	19.2kg	7.5kg	2.59Hz

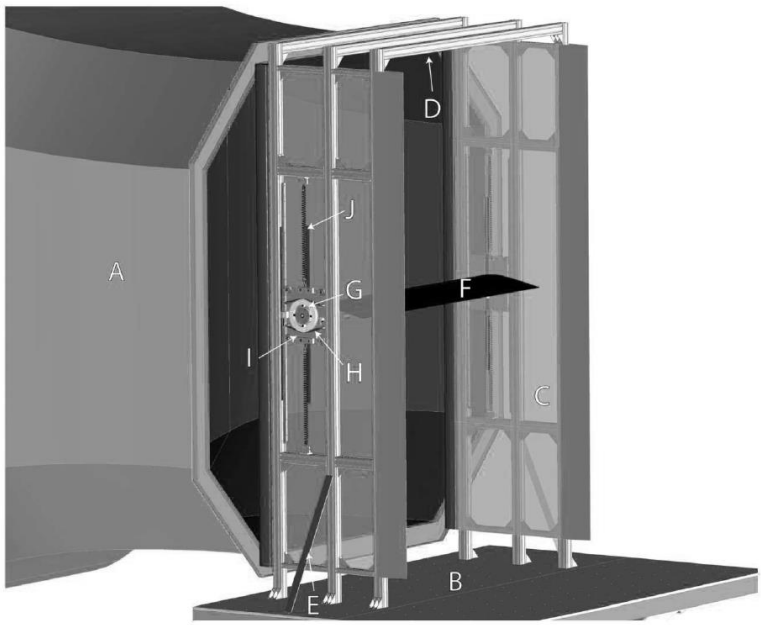

Figure 3. Experimental set-up in open jet facility: the jet exit (A), the table (B), two sides upright (C), connecting beams (D), struts (E) and the wing (F). Moment sensors (G) are attached to springs (H) on movable side plates (I) [11]

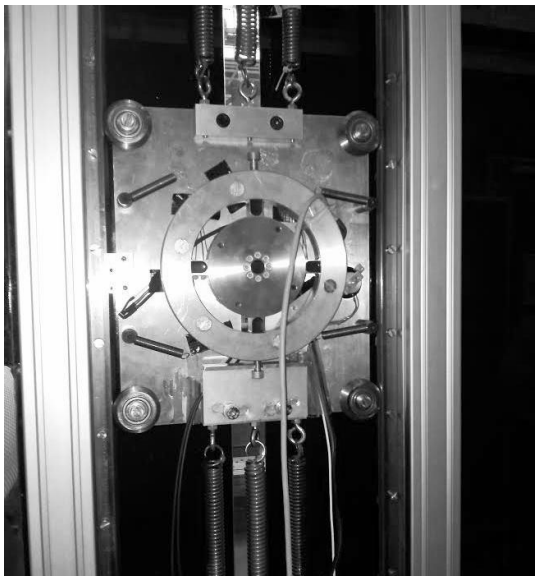

Figure 4. Plunge-pitch mechanism

The original flap, which was driven by an electric motor, has been replaced by a free-floating flap. As the wing is mounted horizontally in the test set-up, gravity plays an important role in the design of the FFF, which does not have any rotational stiffness. A 2D aerodynamic analysis has been carried out in XFoil coupled to a simple 1 degree of freedom model with the flap deflection as degree of freedom. The first mass moment of the flap with respect to its rotational axis and the angle of attack of the airfoil serve as input parameters to this study. Figure 5 displays the resulting flap deflection angles for wind speeds of 10m/s. The isobars represent constant mass moments of the flap around its hinge line. For controllability of the free-floating flap it is important that the flow remains attached and that the aerodynamic response of the wing section remains linear. Therefore it was decided that very high flap deflection angles should be avoided. Since the airfoil is not symmetric, it produces considerable lift even at zero angle of attack. This helps in counteracting gravity and leveling the flap section. When the flap deflection angle is limited to 6 degree, a maximum allowable first mass moment of 25gm can be found. The variation of the flap deflection angle with respect to the angle of attack is rather small and remains within 1 degree over the considered range of angles of attack.

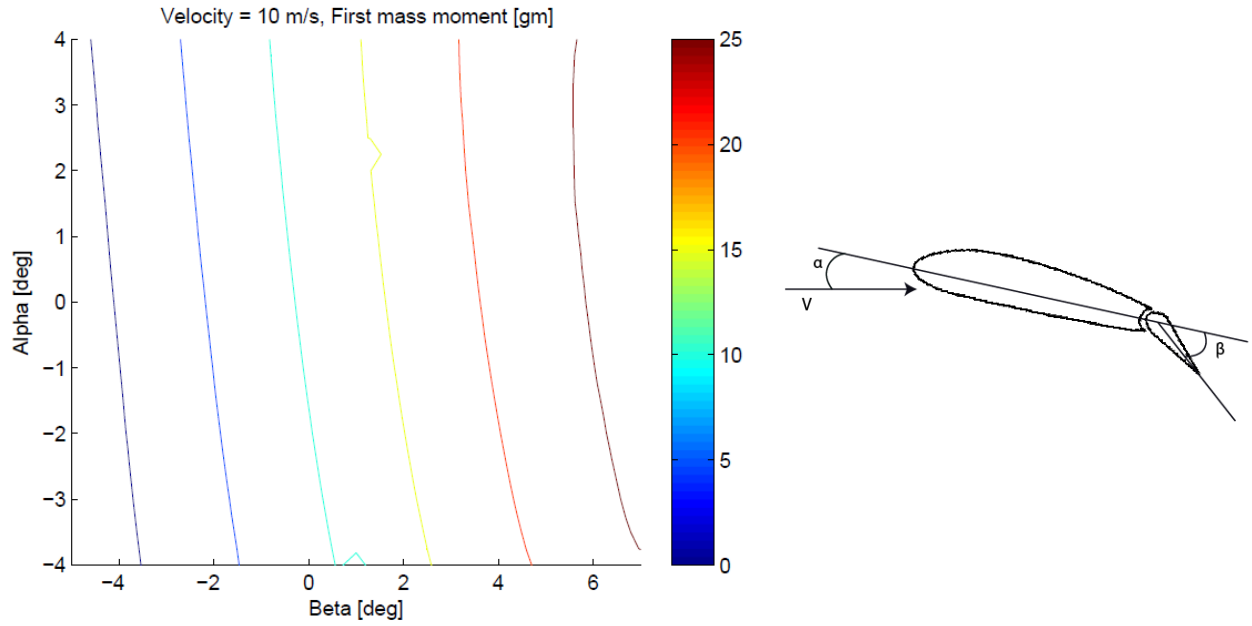

Figure 5. Flap deflection as function of angle of attack and flap mass

4. STABILITY EVALUATION

Both the control authority [2] as well as the potential for energy harvesting [9] increases when approaching flutter speed. Therefore, a stability analysis is crucial for the design of the aeroelastic system. This analysis has been performed using a PK method in MSC Nastran [12]. Compared to the original model as given in Table 1 several modifications have been made to increase the flutter speed. The flutter speed should not be too low since the aerodynamic forces on the flap must be able to overcome friction in the flap hinges and energy harvesting system. To increase the flutter speed two measures are taken. The first one was to increase the spring stiffness in plunge to 15000N/m. The second change lies in the mass

distribution of the flap. It is desirable to achieve a high second mass moment around the hinge axis, while keeping the first mass moment low. This can be realized by adding a counterweight in front of the flap axis. This improves the design twofold. Firstly, the flutter speed is increased, while the violence of its onset is decreased. Secondly, the flap angle in its neutral position is reduced, as shown in Figure 5, as the counterweight will decrease the first mass moment. For the presented design a counterweight of 200g is used per flap.

The eigenmodes are shown in Figure 6. The frequency of the first plunge mode has increased to 3.6Hz compared to 2.59Hz in the original set-up. As both flaps are free-floating, the eigenfrequency of these modes is 0Hz. The 4th considered mode is a pitching mode at 7.6Hz. All of these modes are rigid body modes of the wing assembly and clearly separated from the elastic modes, which have frequencies of an order of magnitude higher.

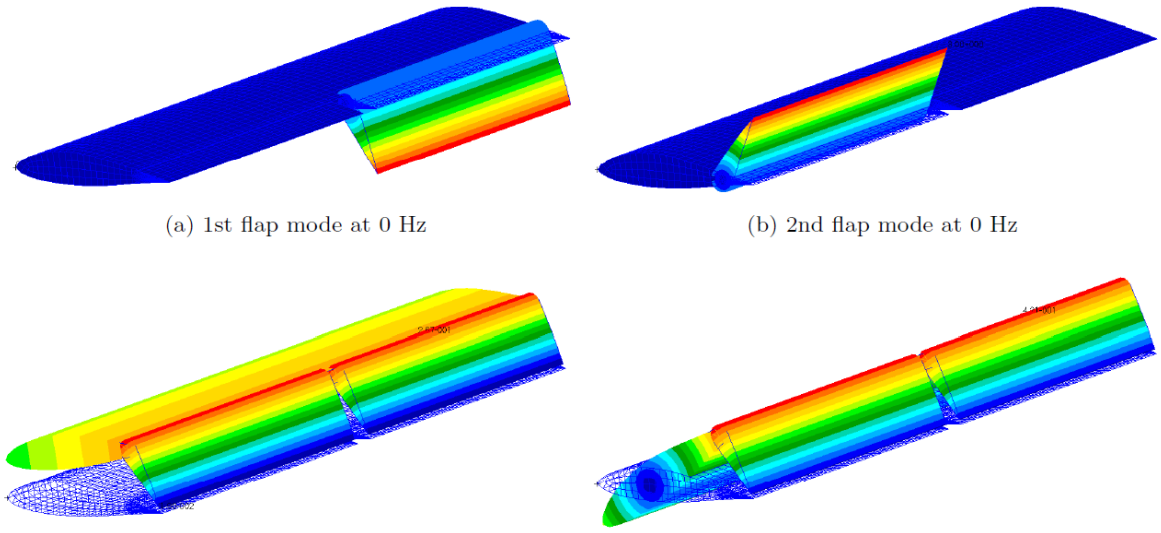

(a) 1st flap mode at 0 Hz

(b) 2nd flap mode at 0 Hz

(c) 1st plunge mode at 3.6 Hz

(d) 1st pitch mode at 7.6 Hz

Figure 6. Structural modes

The frequency and damping plots change according to the model adaptations. As can be seen in Figure 7, the eigenfrequencies are updated. Both rigid body pitch and plunge frequencies are almost independent of the wind speed, while the frequencies of both flaps increases quickly. Already at wind speeds as low as 9m/s the frequencies of the flap modes approach the frequency of the plunge mode. The modes start to interact, which results in the dynamic instability of the plunge mode as displayed in the damping plot in Figure 7. The frequencies of the flap keep increasing beyond the flutter point and eventually will also interact with the pitch mode, however the wind speed at which this occurs is beyond the scope of interest of this research. The amplitude of the flap rotations is structurally limited such that the flap will go into a limit cycle oscillation (LCO).

As a final design step, the mode shapes as obtained by MSC Nastran have been used as basis for an aeroelastic analysis in ZAERO [13]. ZAERO has been used to obtain a state-space representation of the aeroelastic plant. The transfer functions between accelerometers and tab deflection angle have been assessed using the obtained state-space models. The bode plots are given in Figure 8. Both eigenfrequencies of plunge and pitch modes are clearly visible at 3.6Hz and 7.6Hz, respectively. The first elastic eigenfrequency is found back at 37Hz. The acceleration of one of the two flaps is used as sensor. The 2 curves visible in Figure 8 correspond to trailing edge activity on the flap with the sensor and on other flap. For frequencies up to 20 Hz, the responses are identical. This is to be expected as both plunge and pitch motion are symmetric with respect to the midplane. The first elastic mode at 37Hz is the first wing bending mode. As the side plates fix the wing to the frame, rotations at the endpoints are not possible. The resulting mode is therefore S-shaped, meaning that one of side moves upwards, while the other side moves downwards. This motion is skew symmetric. Therefore the amplitude of the response function is identical, but a phase shift between the structural responses due to trim tab deflections on both flaps is introduced.

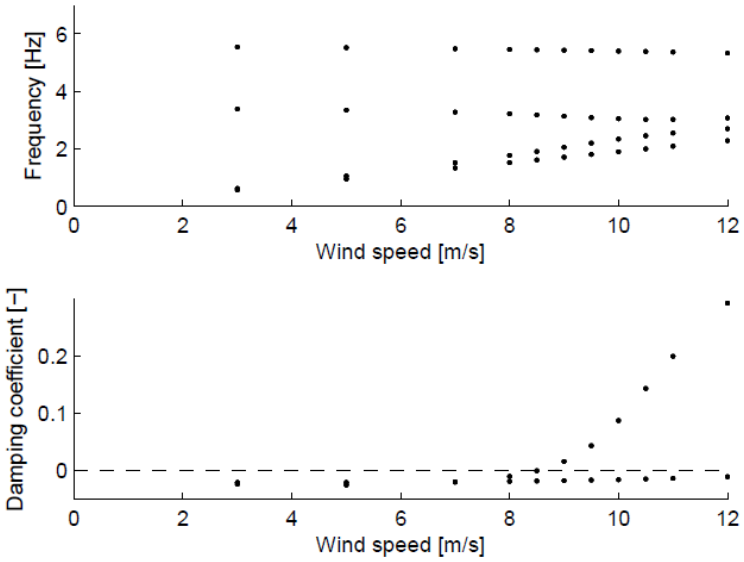

Figure 7. Damping and frequency plots as function of velocity

One should notice that the control authority is reduced compared to previous research [7]. The reason is that a smooth transition between wing and flap is desired. To achieve this, the hinge line has been moved forward to coincide with the end point of the main wing structure. This increases the moment arm to the aerodynamic center of the flap, thereby reducing the effectiveness of the trim tabs. Nonetheless, one degree of trim rotation still translates into 0.5 degrees of flap deflection.

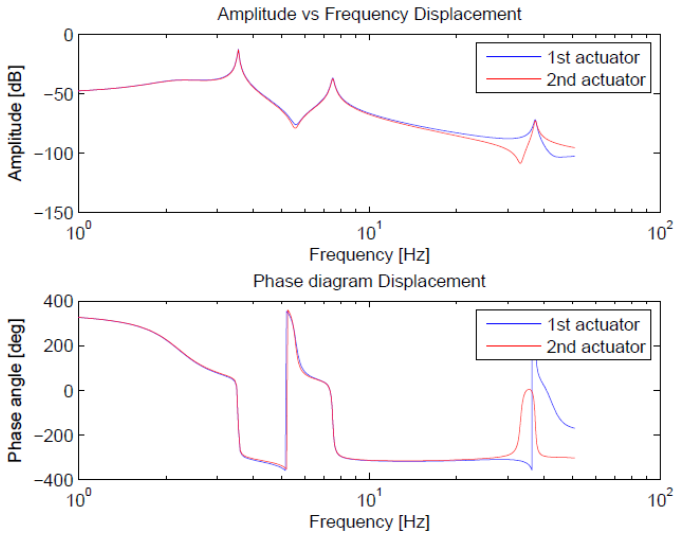

Figure 8. Bode plot of tab deflection to flap rotation

5. PHYSICAL MODEL DESIGN

The physical model of the flap system has been designed based on the requirements derived in the previous section. To keep the set-up simple, of the shelf components have been used as much as possible. The flap structure was printed using stereolithography. The thickness has been kept to a minimum manufacturable thickness of 2mm. The thickness is not driven by loads, but only by manufacturing constraints.

Other components were selected upon suitability for their task. An overview of the components can be found in Table 2. The space at the trailing edge of the flap is very limited, consequently only micro actuators can be implemented. Torque and speed requirements for control of the trailing edge tabs makes servo motors a very suitable solution. HiTec HS 7115^{TH} was selected because of its slenderness. The thickness of 8mm just fits between the upper and the lower skin. The torque of 3.9kgcm is also more than sufficient. The actuator can travel 60 degrees in 0.10 seconds at 7.4V, which can be directly provided by the battery, which suffice for two hours of continuous operation of the servo actuator.

Table 2 Flap design parameters

Material	Density	Young's modulus	Tensile strength	Skin thickness
SL-Tool Stonelike[a]	1.37g/cm^3	3.5GPA	47MPA	2mm
Servo actuator	Gear box	Gear ratio	Generator	Accelerometer
HiTec HS-7115TH[b]	Apyxdyna AM022[c]	1:80	Kinetron MG 23.0[d]	Analogue Devices ADXL78[e]

a. https://www.robotmech.com/uploads/media/robotmech-SL-TOOL-Stonelike_EN.pdf
b. http://hitecrcd.com/products/servos/premium-digital-servos/hs-7115th-hv-ultra-slim-titanium-gear-servo/product
c. http://www.apexdyna.nl/en/producten/am-series.html
d. http://www.kinetron.eu/micro-generator-technology/
e. http://www.analog.com/en/mems-sensors/mems-inertial-sensors/adxl78/products/product.html

Compared to the previous experimental research [10] the hinge axis is connected to a gear box with ratio 1:80 to get the generator close to its optimal working point. The system layout is shown in Figure 9. 2 generators are installed per flap. Their voltage is rectified and together they charge a single battery which is used to power accelerometer and actuators. For convenience, the controller is not integrated in the flap system, but rather connected through a real-time pc, which also serves as data acquisition system.

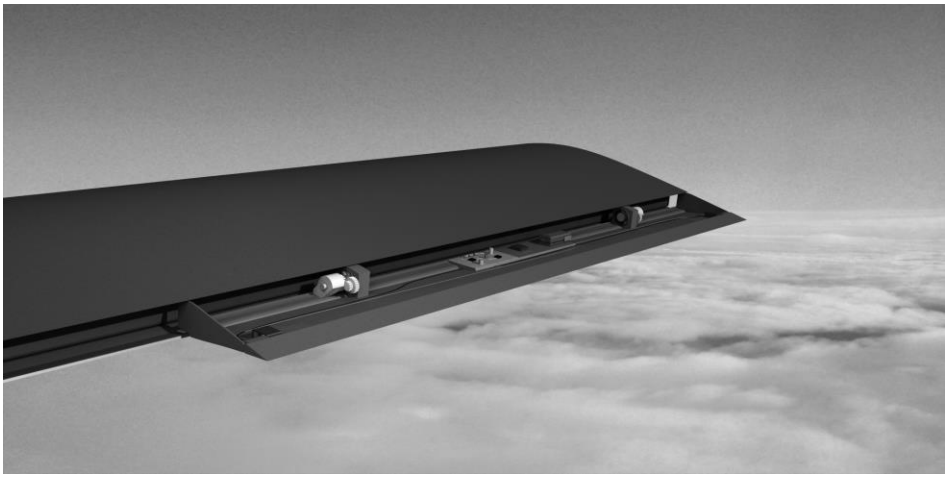

Figure 9. Free-floating flap with active trailing edge

The power requirements are driven by the flap operation. The estimated power consumption during operation is 10.47mW per flap. Each generator can produce up to 70mW at a nominal speed of 800RPM, which is the average rotational speed in LCO. This means that the system can operate 92.8% of the time in a control mode.

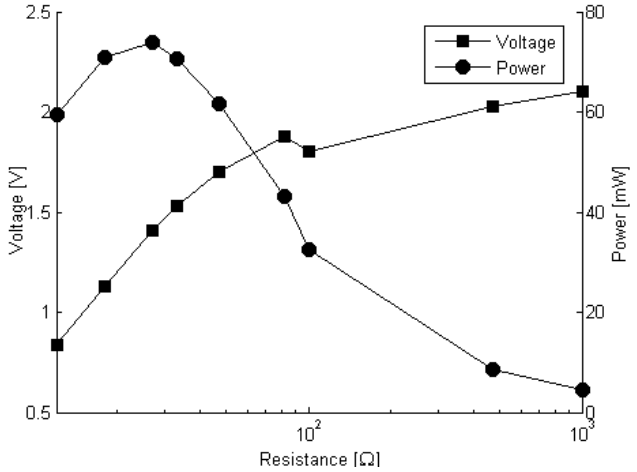

Figure 10. Power and voltage as a function of resistance

During the experiment, a wide variety of parameters will be monitored. First of all, the flap system parameters, including plunge accelerations, flap rotation, charging voltage and battery charge are measured. The trim tab deflection angle is a control input and will be stored synchronously. Besides the measurement devices mounted on the flap, also the structural frame is equipped with sensors. An overview can be found in Table 3. The wind tunnel experiment will be carried out in the open jet facility (OJF) of Delft University of Technology. The open jet facility is a closed circuit tunnel with a test section of 2.85m by 2.85m. Wind speeds up to 35 m/s can be reach, which corresponds to a Reynolds number of 1,230,000 based on a 50cm chord. The Reynolds number at the predicted flutter speed is 320,000.

Table 3 Sensors on frame

Load cell	Strain gauges	Moment sensor	Displacement sensor	Potentiometer
FLB3G	LY41-6-350	TS170	TM10E	LNB22

5. CONCLUSION

In this paper the design of an aeroelastic technology demonstrator has been outlined. The novel concept of the autonomous flap is based on a self-controlled, self-powered flap. It can be used for load alleviation purposes. The flap concept is applied to an already existing aeroelastic test bench. Flutter predictions show that the system will become instable at 9 m/s. This instability will transition into limit cycle oscillation as a result of structural delimiters. The energy of these oscillations is converted into electrical energy, which can serve as power source of the trailing edge tabs that are used to control the free-floating flaps.

REFERENCES

1. Heinze, S. and Karpel, M., "Analysis and wind tunnel testing of a piezo-electic tab for aeroelastic control applications," *Journal of Aircraft*, Vol. 43, No. 6, 2006, pp. 1799-1804.
2. Bernhammer, L., De Breuker, R., Karpel, M., and van der Veen, G., "Aeroelastic Control Using Distributed Floating Flaps Actuated by Piezoelectric Tabs," *Journal of Aircraft*, Vol. 50, No. 3, 2013, pp. 732-740.
3. Pustilnik, M. and Karpel, M., "Dynamic Loads Alleviation Using Active Free-Floating Flaps," *Proceedings of 53rd Israel Annual Conference on Aerospace Sciences*, Haifa, Israel, 2013.
4. Pustilnik, M. and Karpel, M., "Loads, Vibration and Maneuver Control Using Active Floating Flaps," *Proceedings of International Forum on Aeroelasticity and Structural Dynamics*, Royal Aeronautical Society, Bristol, UK, 2013.
5. Bryant, M. and Garcia, E., "Modeling and Testing of a Novel Aeroelastic Flutter Energy Harvester," *Journal of Vibration and Acoustics*, Vol. 133, 2011, pp. 011010-1:10.
6. Bryant, M., Fang, A., and Garcia, E., "Self-powered smart blade: Helicopter blade energy harvesting," *Proceedings of the SPIE*, Vol. 7643, 2010, pp. 764317-1:10.
7. Park, J., Kim, K., Kwon, S., and Law, K. H., "An aero-elastic utter based electromagnetic energy harvester with wind speed augmenting funnel," *Proceedings of Int. Conference on Advances in Wind and Structures*, KAIST, Seoul, Korea, 2012.
8. Park, J., Morgenthal, G., Kim, K., Kwon, S., and Law, K. H., "Power Evaluation for Flutter-Based Electromagnetic Energy Harvester using CFD Simulations," *Proceedings of First International Conference on Performance-based and Life-cycle Structural Engineering*, Hong Kong, China, 2012.
9. Bernhammer, L., De Breuker, R., and Karpel, M., "Energy Harvesting for Sensors using Free-Floating Flaps," *Proceedings of 24th International Conference on Adaptive Structures and Technologies*, Aruba, 2013.
10. Bernhammer, L., De Breuker, R., and Karpel, M., "Energy Harvesting for Sensors using Free-Floating Flaps: Wind Tunnel Experiments," *Proceedings of 54th Israel Annual Conference on Aerospace Sciences*, Tel Aviv, Israel, 2014.
11. Sterenborg, J., Experimental and numerical investigation of an aeroelastic wing, TU Delft, 2014, PhD Thesis.
12. Rodden, W. and Johnson, E., "MSC Nastran Aeroelastic Analysis User's Guide," MSC. Software Corporation USA, 1994.
13. Zona Technology, "ZAERO Theoretical Manual". Scottsdale, USA, 2011.